

International Journal of Modern Physics A
 © World Scientific Publishing Company

HADRONS ABOVE T_c

TETSUO HATSUDA

*Department of Physics, University of Tokyo,
 Tokyo, 113-0033, Japan*

Received (Day Month Year)

Revised (Day Month Year)

Hadronic modes in the quark-gluon plasma and their spectral properties are discussed on the basis of the lattice QCD data.

Keywords: quark-gluon plasma; lattice QCD; charmonium.

1. Introduction

Fate of light hadronic excitations above the critical temperature T_c of the QCD phase transition was first investigated 20 years ago.^{1,2}

In Ref. 1 whose title is “Fluctuation effects in hot quark matter: precursors of chiral transition at finite temperature”, the hadronic modes above T_c were discussed in connection with the critical fluctuation associated with chiral symmetry restoration: The abstract says “... *there arise soft modes having a large strength and a narrow width above the critical temperature, which are analogous to the fluctuation of the order parameter in a superconductor above the critical point.*” An example of such soft mode (σ - π) at $T > T_c$ was demonstrated using the Nambu-Jona-Lasinio model^{1,3} and was later called the “para-pion”.⁴ From the modern point of view, it could be identified as a pre-formed $q\bar{q}$ resonance in the pseudo-gap phase where the chiral order parameter has a large fluctuation above T_c (see e.g. Refs. 5, 6).

In Ref. 2 whose title is “Conjecture concerning the modes of excitation of the quark-gluon plasma”, the hadronic modes above T_c were discussed with a different perspective which is unique in non-Abelian gauge theories, i.e. the dynamical confinement of the plasma above T_c : The abstract says “... *the plasma exhibits confining features similar to that of the low-temperature hadronic phase. The confining features are manifest in the long-range, i.e., long-wavelength, low-frequency, modes of the plasma.*”

Recently, studies of the hadronic modes in the time-like domain become possible in lattice QCD simulations owing to the technique of the maximum entropy method (MEM).^{7,8} It was then found that some hadronic modes (in the $s\bar{s}$ sector) survive even at $T > T_c$ in quenched simulations (see Sec. 4).⁹ However, its relation to the

2 *Tetsuo Hatsuda*

above ideas (chiral pseudo-gap or dynamical confinement) is not yet clear.

For heavy hadrons such as the charmonia, it has been considered that they dissolve soon after the deconfinement because the screened Coulomb potential above T_c is not strong enough to hold the $c\bar{c}$ pair.^{10,11} However, the quenched lattice QCD simulations^{12,13,14} have recently shown that resonances such as J/Ψ and η_c survive even up to $T/T_c \sim 1.6$ (see Sec. 4). Physical origin of this phenomena is also an open question at the moment.

2. QCD spectral functions and MEM

The Matsubara correlation in a mixed representation is defined as $D(\tau, \mathbf{p}) = \int d^3x \mathcal{D}(\tau, \mathbf{x}) e^{-i\mathbf{p}\cdot\mathbf{x}}$, where $\mathcal{D}(\tau, \mathbf{x})$ is the imaginary time two-point function. The spectral representation tells

$$D(\tau, \mathbf{p}) = \int_{-\infty}^{+\infty} \frac{e^{-\tau\omega}}{1 \mp e^{-\beta\omega}} A(\omega, \mathbf{p}) d\omega \quad (0 \leq \tau < \beta), \quad (1)$$

which is convergent for $\tau \neq 0$ in QCD. $A(\omega, \mathbf{p})$ contains all the information of hadronic modes (mass, width etc) in the relevant channel.

Reconstructing a continuous function $A(\omega, \mathbf{p})$ from discrete and finite lattice data $D(\tau, \mathbf{p})$ is a typical ill-posed problem. One way to avoid this difficulty is to introduce an ansatz for the spectral function with a few parameters.¹⁵ The maximum entropy method (MEM) provides an alternative and much more powerful approach^{8,16}: one can obtain a unique A from the lattice data D without making a priori parameterizations. Also, statistical significance of the resultant A can be evaluated.

In MEM, the most probable A given lattice data D is obtained by maximizing the conditional probability $P[A|D] \propto e^{\alpha S - L}$, where L is the standard likelihood function and S is the Shannon-Jaynes information entropy:

$$S = \int_0^\infty \left[A(\omega) - m(\omega) - A(\omega) \log \left(\frac{A(\omega)}{m(\omega)} \right) \right] d\omega. \quad (2)$$

The statistical significance (error) of the resultant A is estimated by the second variation, $(\delta/\delta A)^2 P[A|D]$. The default model $m(\omega)$ in Eq.(2) may be chosen so that the MEM errors become minimum. The final result is given by a weighted average over the parameter α as $A(\omega, \mathbf{p}) = \int A_\alpha(\omega, \mathbf{p}) P[\alpha|Dm] d\alpha$, where $A_\alpha(\omega, \mathbf{p})$ is obtained by minimizing $P[A|D]$ for a fixed α .

First successful application of MEM to the lattice QCD data at $T = 0$ was carried out for the ground and excited mesons in Ref. 7. Also, basic concepts and techniques of MEM applied to lattice QCD are summarized in Ref. 8.

3. Applications of MEM ($T = 0$)

Shown in the left panel of Fig. 1 is a spectral image of the vector meson at rest ($\mathbf{p} = 0$) extracted from the quenched QCD data.⁷ The first (second) peak corresponds to

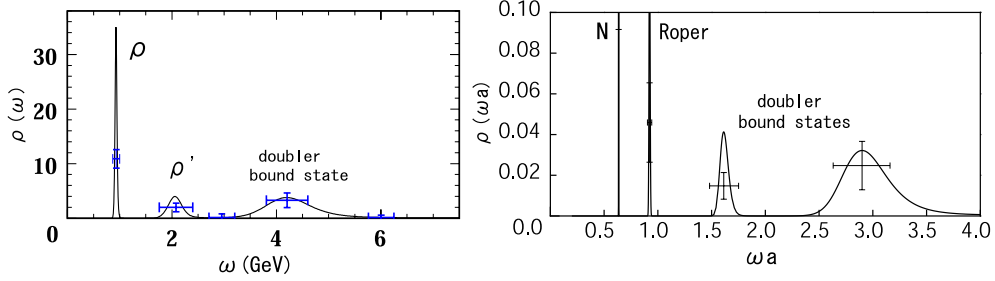


Fig. 1. Left panel: The dimensionless spectral function $\rho(\omega) = A(\omega, \mathbf{0})/(3\omega^2)$ of the vector meson extracted from a $20^3 \times 24$ lattice with $\beta = 6.0$. The hopping parameter is take to be $\kappa = 0.1557$. The figure is adapted from Ref. 7. Right panel: The dimensionless spectral function $\rho(\omega) = A(\omega, \mathbf{0})/\omega^5$ in the nucleon channel extracted from a 32^4 lattice with $\beta = 6.0$ ($a \simeq 0.093$ fm). The hopping parameter is take to be $\kappa = 0.1550$. The horizontal axis denotes a dimensionless frequency ωa . This figure is adapted from Ref. 18.

the ground (excited) vector meson. On the other hand, the highest peak corresponds to a bound state of Wilson doublers as first pointed out in Ref. 17. Shown in the right panel of Fig. 1 is the spectral function in the nucleon channel extracted from the quenched QCD data.¹⁸ The first (second) peak corresponds to the nucleon and the Roper resonance, while the higher two peaks correspond to the bound states of Wilson doublers.

4. Applications of MEM ($T \neq 0$)

In Refs. 9, 12, quenched QCD simulations with $\beta = 7.0$ on $32^3 \times N_\tau$ anisotropic lattice were performed using naive plaquette gauge action and the standard Wilson quark action. The renormalized anisotropy is $\xi = a_\sigma/a_\tau = 4.0$ with $a_\tau = a_\sigma/4 = 9.75 \times 10^{-3}$ fm and $L_\sigma = 1.25$ fm. Employing the anisotropic lattice is necessary to keep the number of temporal data points as large as possible; N_τ is taken to be 96, 54, 46, 44, 42, 40 and 32 which correspond to $T/T_c = 0.78, 1.38, 1.62, 1.70, 1.78, 1.87$ and 2.33 , respectively.

$s\bar{s}$ mesons at $T \neq 0$

Shown in Fig.2 is the spectral functions of the $s\bar{s}$ mesons in the scalar (S), pseudo-scalar (PS), vector (V) and axial-vector (AV) channels for $T/T_c = 1.38$.⁹ The quark mass is chosen to reproduce the experimental ϕ meson mass at $T = 0$ approximately. One finds that spectral functions in all channels have degenerate peaks around 2.5 GeV at $T/T_c = 1.38$ (2.4 times the ϕ -meson mass at $T = 0$). Also, these peaks have been shown to disappear at higher temperatures e.g. at $T/T_c = 1.87$.⁹

$c\bar{c}$ mesons at $T \neq 0$

Shown in Fig.3 is the case for charmonia.¹² Quark masses are chosen so that we have $m_{J/\psi}^{\text{lat}} \simeq 3.10\text{GeV}$ and $m_{\eta_c}^{\text{lat}} \simeq 3.03\text{GeV}$ at $T = 0$, which should be compared

4 Tetsuo Hatsuda

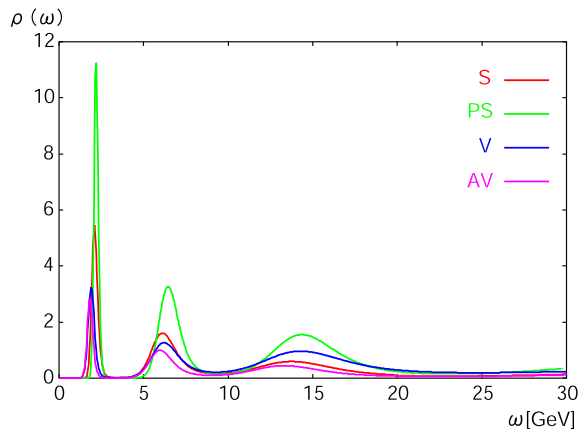


Fig. 2. The dimensionless spectral function measured on an anisotropic lattice for the $s\bar{s}$ mesons at $T/T_c = 1.38$. The figure is taken from Ref. 9.

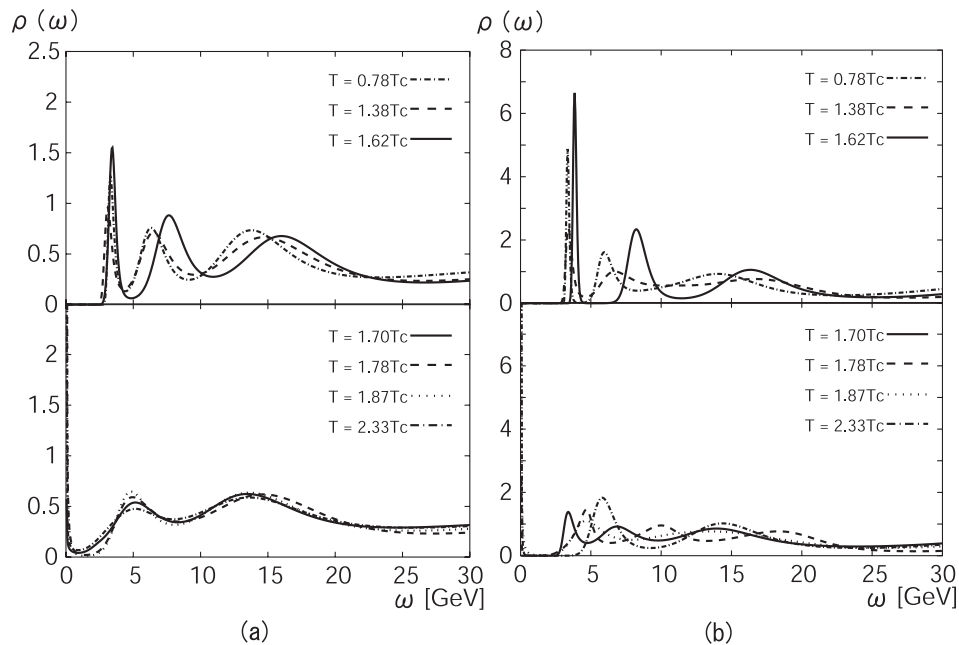


Fig. 3. Spectral functions measured on an anisotropic lattice for (a) the J/Ψ channel ($\rho(\omega) = A(\omega, \mathbf{0})/(3\omega^2)$) and for (b) the η_c channel ($\rho(\omega) = A(\omega, \mathbf{0})/\omega^2$). Figures adapted from Ref. 12.

with the experimental values, 3.10 GeV and 2.98 GeV, respectively.

Sharp peaks for J/Ψ and η_c are found even up to $T \simeq 1.62T_c$ as shown in Fig.3 with the peak position almost the same as their $T = 0$ values. Similar observations on the charmonium bound states above T_c were obtained in other independent

studies.^{13,14} In our case, the sharp peaks disappear suddenly between $1.6T_c$ and $1.7T_c$. The width of the first peak in Fig.3 partly reflects the unphysical broadening due to the statistics of the lattice data and partly reflects possible physical broadening at finite T . The second and third peaks in Fig.3 are likely to be related to Wilson doublers.

reliability of the MEM images

Lack of accurate lattice data can cause fake peaks and/or fake smearing as demonstrated by the mock data in Ref. 8. Therefore the spectral functions obtained from MEM should pass some reliability tests. The first test is the error analysis of the peaks from the second variation, $\delta^2 P[A|D]/\delta A(\omega)\delta A(\omega')$. The second test is the change of the spectral functions under the variation of the number of data point N_{data} employed for the MEM analysis. The third test is a study of the finite volume effect in the spatial direction. The results in Fig.3 have already passed the first and second tests. An attempt toward the third test is recently reported in Ref. 19.

effects of dynamical quarks

If dynamical quarks are included, there arise two competing effects to the dissociation rate of the hadronic modes observed in the quenched simulations: enhancement due to collisions with dynamical quarks, and suppression due to small critical temperature in full QCD ($T_c^{\text{quench}} \sim 270$ MeV vs. $T_c^{\text{full}} \sim 170$ MeV). The number ratio of the plasma constituents between full QCD ($N_f = 2$) and quenched QCD ($N_f = 0$) reads

$$\frac{n_{q+g}(T_c^{\text{full}})}{n_g(T_c^{\text{quench}})} = \frac{16 + 21}{16} \cdot \left(\frac{T_c^{\text{full}}}{T_c^{\text{quench}}} \right)^3 \simeq 0.62. \quad (3)$$

Therefore, the net thermal dissociation rate of the hadronic resonances may be even smaller in full QCD than that in quenched QCD for given T/T_c . In any case, it is truly necessary to carry out full QCD simulations to make definite conclusions. A preliminary study in $N_f = 2$ QCD is recently reported in Ref. 20.

5. Concluding remarks

In this report, we have discussed the old idea of hadronic modes above T_c (chiral pseudo-gap¹ and dynamical confinement²) and recent quenched lattice QCD results showing the existence of resonance structures above T_c in $s\bar{s}$ and $c\bar{c}$ channels. To unravel the true nature of such hadronic modes above T_c , it is important to extract more information from lattice QCD data, such as the spatial wave functions,²¹ spectral functions with finite spatial momentum,²² role of hadronic modes to bulk plasma properties,²³ and $q\bar{q}$ and q - g potentials above T_c .²⁴ Further theoretical studies on the possible mechanisms^{25,26} to support hadronic states above T_c are also called for.

6 *Tetsuo Hatsuda*

Acknowledgments

This work was supported by Grants-in-Aid of the Japanese Ministry of Education, Culture, Sports, Science and Technology, No. 15540254.

References

1. T. Hatsuda and T. Kunihiro, Phys. Rev. Lett. **55**, 158 (1985).
2. C. DeTar, Phys. Rev. D **32**, 276 (1985).
3. T. Hatsuda and T. Kunihiro, Phys. Rept. **247**, 221 (1994).
4. T. Hatsuda, hep-ph/9502345.
5. E. Babaev, Phys. Rev. D **62**, 074020 (2000); Int. J. Mod. Phys. A **16**, 1175 (2001).
6. M. Kitazawa, T. Kunihiro and Y. Nemoto, hep-ph/0505106.
7. Y. Nakahara, M. Asakawa and T. Hatsuda, Phys. Rev. D **60**, 091503 (1999).
8. M. Asakawa, T. Hatsuda and Y. Nakahara, Prog. Part. Nucl. Phys. **46**, 459 (2001).
9. M. Asakawa, T. Hatsuda and Y. Nakahara, Nucl. Phys. Proc. Suppl. **119**, 481 (2003); Prog. Theor. Phys. Suppl. **149**, 42 (2003).
10. T. Hashimoto, K. Hirose, T. Kanki and O. Miyamura, Phys. Rev. Lett. **57**, 2123 (1986).
11. T. Matsui and H. Satz, Phys. Lett. B **178**, 416 (1986).
12. M. Asakawa and T. Hatsuda, Phys. Rev. Lett. **92**, 012001 (2004); J. Phys. **G30**, S1337 (2004).
13. T. Umeda, K. Nomura and H. Matsufuru, Eur. Phys. J. **C 39S1**, 9 (2005).
14. S. Datta, F. Karsch, P. Petreczky and I. Wetzorke, Phys. Rev. **D69**, 094507 (2004).
15. T. Hashimoto, A. Nakamura and I.O. Stamatescu, Nucl. Phys. **B400**, 267 (1993); *ibid.* **B406**, 325 (1993).
16. M. Jarrell and J.E. Gubernatis, Phys. Rep. **269**, 133 (1996).
17. T. Yamazaki et al. (CP-PACS Collaboration), Phys. Rev. **D65**, 014501 (2002).
18. K. Sasaki, S. Sasaki and T. Hatsuda, Phys. Lett. **B623**, 208 (2005).
19. H. Iida, N. Ishii, T. Doi and H. Suganuma, hep-lat/0509129.
20. R. Morrin et al., A. P. Ó Cais, M. B. Oktay, M. J. Peardon, J. I. Skullerud, G. Aarts and C. R. Allton, hep-lat/0509115.
21. Ph. de Forcrand et al. (QCD-TARO Collaboration), Phys. Rev. **D63**, 054501 (2001).
22. S. Datta, F. Karsch, S. Wissel, P. Petreczky and I. Wetzorke, hep-lat/0409147.
G. Aarts, S. Hands, S. Kim and J. M. M. Resco, hep-lat/0509062.
23. S. Ejiri, F. Karsch and K. Redlich, hep-ph/0509051.
S. Ejiri and T. Hatsuda, hep-lat/0509119.
24. A. Nakamura and T. Saito, Prog. Theor. Phys. **111**, 733 (2004); *ibid.* **112**, 183 (2004).
25. G. E. Brown, C.-H. Lee, M. Rho, E. Shuryak, Nucl. Phys. **A740**, 171 (2004).
E. Shuryak and I. Zahed, Phys. Rev. **D70**, 054507 (2004).
Y. A. Simonov, Phys. Lett. **B619**, 293 (2005).
26. S. Digal, P. Petreczky and H. Satz, Phys. Lett. **B514**, 57 (2001).
C. Y. Wong, hep-ph/0408020.
S. Digal, O. Kaczmarek, F. Karsch and H. Satz, hep-ph/0505193.
W. M. Alberico, A. Beraudo, A. De Pace and A. Molinari, hep-ph/0507084.